Equilibrium and Growth Morphology of Oligoacenes: Periodic Bond Chains (PBC) Analysis of Tetracene Crystal

ARTICLE *in* CRYSTAL GROWTH & DESIGN · OCTOBER 2011

Impact Factor: 4.89 · DOI: 10.1021/cg200924m

5 AUTHORS, INCLUDING:

Francesco Roberto Massaro
University of Padova
41 PUBLICATIONS **286** CITATIONS
SEE PROFILE

Marco Bruno
Università degli Studi di Torino
84 PUBLICATIONS **704** CITATIONS
SEE PROFILE

Marco Rubbo
Università degli Studi di Torino
98 PUBLICATIONS **608** CITATIONS
SEE PROFILE

Dino Aquilano
Università degli Studi di Torino
190 PUBLICATIONS **992** CITATIONS
SEE PROFILE

CRYSTAL GROWTH & DESIGN

ARTICLE

pubs.acs.org/crystal

Equilibrium and Growth Morphology of Oligoacenes: Periodic Bond Chains (PBC) Analysis of Tetracene Crystal

Francesco Roberto Massaro,*[,†] Massimo Moret,[†] Marco Bruno,[‡] Marco Rubbo,[‡] and Dino Aquilano[‡]

[†]Dipartimento di Scienza dei Materiali, Università di Milano Bicocca, via R. Cozzi 53, I-20125 Milano, Italy

[‡]Dipartimento di Scienze Mineralogiche e Petrologiche, Università di Torino, via Valperga Caluso 35, I-10125 Torino, Italy

Supporting Information

ABSTRACT: The athermal equilibrium and growth shapes of tetracene crystal were calculated, in a vacuum, by using computer codes (CSEHP, GULP, and TINKER) along with three different sets of empirical potentials (UNI, UFF, and MM3 force fields). The surface profiles were obtained by applying the Hartman−Perdok method of the periodic bond chains (PBC). The specific surface and attachment energy values were calculated, both for ideal and relaxed surface profiles. From calculations, it follows that the equilibrium shape of tetracene shows a nearly barrel habit: one form, the {001}, rules over the other ones, and several faces roughly belong to the zone axis perpendicular to the dominant form. Concerning the growth morphology, a plate-like habit with the dominant pinacoid is obtained. An excellent agreement among the three force fields employed was observed. A relevant result emerging from this work is the observation that surface relaxation in general weakly affects surface and attachment energies of molecular crystals.

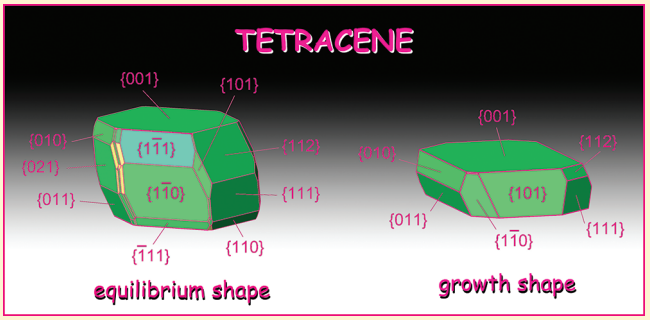

1. INTRODUCTION

Organic π-conjugated organic molecules are intensively investigated in order to ascertain whether they can represent a valid substitute for inorganic semiconductors.[1−4] Studies on these organic materials involve both single crystals and thin films, allowing researchers to study the material's intrinsic properties and the possibility to build fully operating devices, respectively. In this respect, one of the most critical issues is crystal morphology, that is, the collection of faces that bound the macro- or microcrystalline samples. In fact, surface properties and crystal morphology are both relevant in determining the material's manipulability and its potential exploitation. For example, the film morphology of the donor/acceptor heterostructures used in most organic photovoltaics is a critical variable that rules both the performance of new materials obtained in the lab and the efforts to move them to factory-scale production. Although efficiencies of organic solar cells have improved significantly in recent years, very few accurate studies on crystal morphology were performed, and the morphological optimization of these materials mainly occurs by trial and error. Moreover, morphology can heavily hamper the practical study or use of a selected molecule because of unavailability of suitable faces for studying anisotropy of physical properties of single crystals or due to performance degradation in thin films, for example, charge carrier mobilities dependence upon grain boundaries. In the case of thin films the physicochemical situation is even more complicated due to the presence of a suitable (organic or inorganic) substrate with its own interactions (epitaxial or not) with the organic semiconductor crystalline phase.

Therefore, the extensive work dedicated in recent years to organic semiconductors includes improved methods to grow high-quality single crystals and thin films. This step necessarily requires a deep knowledge of the intrinsic properties of the material, first of all the role exerted by the crystal structure on determining the final morphology. Recently, a few papers have dealt with the simulation of crystal morphology and surface energies for some organic semiconductors belonging to the oligoacenes, oligothiophenes, and polyphenylenes classes.[5−8] The most recent paper[8] treated surface energy and equilibrium crystal morphology of an extensive series of molecules covering several oligomers for each of the cited three chemical classes. It analyzes the crystals by means of the density-functional theory, including nonlocal correlations, to account for the van der Waals interactions. However, despite the highly sophisticated computational methods used to treat the weak intermolecular interactions, the aforementioned approaches for determining the equilibrium crystal morphologies are heavily biased by an a priori choice of few low indexes crystal faces. This strong assumption leads to quite simple predicted morphologies for all the different classes of compounds. At variance, we report here the results of a

Received: July 18, 2011
Revised: August 5, 2011
Published: August 05, 2011

classical analysis based on the periodic bond chain (PBC) theory after Hartman and Perdock,[9−11] assisted by simple and computationally cheap empirical atom−atom potentials. This approach allowed us to thoroughly analyze and classify the intermolecular interactions together with the character of crystal faces according to the PBC theory, eventually leading to a prediction of the equilibrium but also of the growth crystal morphology. As a first case study, we chose the classical organic semiconductor tetracene which is among the most studied organic systems for its semiconductor performance. As a corollary, some suggestions are presented for general application of the proposed method to molecular crystals.

2. COMPUTATIONAL DETAILS

We made use of different computer codes along with three different sets of empirical potentials for verifying the adequacy of the performed calculations, thus obtaining different energetic quantities that are not all available from experiments. The choice of the adopted force fields was suggested by the necessity to operate with potential functions of general effectiveness, since their parameters were obtained by fitting data for a variety of organic compounds. The three codes adopted are described immediately below.

2.1. CSEHP. The crystal site energy according to Hartman and Perdok (CSEHP)[12,13] program is a homemade code. It allows one to obtain a range of noteworthy quantities concerning every kind of crystal, for example, the lattice energy, the specific surface energy (γ_{hkl}) of a $\{hkl\}$ crystal form, the $\{hkl\}$ slice energy, the attachment energy (E_{att}^{hkl}), the specific edge energy (ρ_{uvw}^{hkl}) along a $[uvw]$ crystal direction on a given (hkl) face, the adsorption energies on surfaces or edges, and the end chain energy (ECE) for each periodic bond chain (PBC) of the crystal.

We chose to include in our code the UNI[14,15] force field, principally to calculate the molecular interactions, the ECE of the PBCs, and the γ_{hkl} values.

The ECE is the energy released when a molecule enters, in a crystallographic position, at one end of a semi-infinite PBC. As an example, for a given PBC made by the sequence of building units ... ABABAB...:

$$\mathrm{ECE} = {}^1/_2[{}^1/_2(E_{\mathrm{PBC}} + E_{\mathrm{AB}}) + E_{\mathrm{BU}}]$$

where

- E_{PBC} represents the interaction energy between the AB pair and the remaining part of the semi-infinite chain
- E_{AB} is the interaction energy between two consecutive building units (A and B)
- E_{BU} is the formation energy of the considered building unit.

Hence, the ECE values rank the hierarchy of the strength of the PBCs of a crystal.

Within CSEHP, a crystal is built from a stacking of slices of d_{hkl} thickness fulfilling the systematic extinction rules due to the crystal space group. To calculate a given γ_{hkl} value, CSEHP divides the crystal in two parts, along a given profile of the face. The lower part is a semi-infinite crystal, while the upper part is made by a semi-infinite column whose basis coincides with the two-dimensional (2D) elementary cell of the d_{hkl} slice whose area is A_{hkl}.

If E_j represents the interaction energy between the content of the first upper unit cell with the jth underlying d_{hkl} layer, it is easy to show that the specific surface energy reads:

$$\gamma_{hkl} = (E_1 + 2E_2 + 3E_3 + \ldots)/2A_{hkl} = \sum_{j=1}^{\infty}(jE_j)/2A_{hkl}$$

Only the unrelaxed surface energies are calculated, as CSEHP does not allow the optimization of the surface structure.

2.2. GULP. Other calculations, mainly optimizations of slab geometries and surface energy estimates, were carried out by using the UFF[16] molecular potentials implemented in the General Utility Lattice Program (GULP 3.4)[17] simulation code. In turn, this is based on force field methods and allows foreseeing both structures and properties of crystals from a given set of potentials.

Bulk and slab geometry optimizations were performed by means of the Newton−Raphson method and were considered converged when the gradient tolerance and the function tolerance (*gtol* and *ftol* adimensional parameters in GULP) were smaller than 0.0001 and 0.00001, respectively.

All the surfaces were studied by using the 2D-slab model;[18] *hkl* slabs of varying thickness were generated by separating the bulk structure along the plane of interest. Calculations were performed by considering the original 1 × 1 surface cell and the slab subdivided into two regions:

- region 1, containing both the surface and the underlying layers that are allowed to relax
- region 2, having the same number of layers as region 1 and containing the rest of the slab material where no relaxation, with respect to the bulk crystal structure, is assumed to occur.

Calculations were done by considering slabs with thickness up to 12 layers (six for each region), which are sufficient to reproduce bulk-like properties at the center of the slab and to obtain a careful description of the surface.

According to the standard two-regions strategy[19] employed by GULP, γ_{hkl} values were evaluated from the energy of the surface block (U_s, region 1) and the energy of a portion of bulk crystal (U_b, region 2) containing the same number of atoms as the surface block. Both energies have been referred to A_{hkl}, the common surface area of the primitive unit cell:

$$\gamma_{hkl} = (U_s - U_b)/A_{hkl}$$

Evaluating the surface energy values and successively applying the Gibbs−Wulff theorem[20] allows us to draw the theoretical equilibrium shape (ES) of a crystal. The attachment energy, E_{att}^{hkl}, is on the contrary needed to predict the theoretical growth shape of a crystal. This is the energy released when a stoichiometric layer of material is added on to the surface cut:

$$E_{\mathrm{att}}^{hkl} = U_{\mathrm{tot}}^{n+1} - U_{\mathrm{tot}}^{n} - U_{\mathrm{tot}}^{1}$$

where U_{tot}^{n} represents the total internal energy of a surface model consisting of n growth layers, and U_{tot}^{1} is the energy of the growth layer alone. In practice, the calculation of this exothermic quantity is obtained from the interaction energy of the growth layer at the surface with the rest of the underlying structure. While the attachment energy can be obtained from a single calculation, the surface energy arises from a multistage process, the progressive addition of layers until convergence of γ_{hkl} is reached.

2.3. TINKER. The last set of our simulations were based on the MM3 force field[21,22] and were carried out with the TINKER 4.2 molecular modeling package[23] which allows optimization of slab geometries and surface energy calculations. The Newton minimization was used with a rms gradient equal to 0.0001 kcal mol^{-1} Å^{-1} and a 45 Å cutoff value for the van der Waals interactions.

The lattice parameters were optimized by means of the Xtalmin program included in the TINKER package. The surfaces were obtained by cutting the optimized bulk structure, according to the *hkl* planes of interest, and the calculations were performed by adopting simple 1 × 1 2D surface cells. No supercells have been used in our calculations.

The 3D slab model we used consists of slabs of selected thickness stacked along a given direction and separated by vacuum gaps large enough for the van der Waals interactions between slabs to be negligible (i.e., beyond the cutoff value). For the calculation of the γ_{hkl}, we adopted

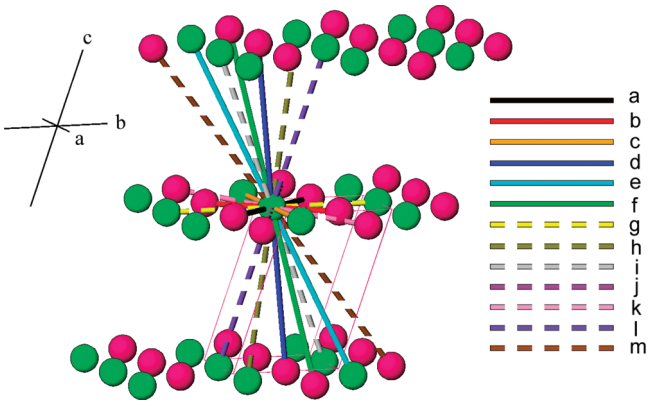

Figure 1. The first and second bond order graph describing the crystal structure of tetracene. Intermolecular bonds are defined in Table 1. The scheme reflects the portion of crystal structure (27 unit cells) considered to estimate the molecular interactions.

the relation:

$$\gamma_{hkl} = (E_s - E_b)/2A_{hkl}$$

where E_s is the optimized slab energy, E_b is the energy of an equivalent number of fixed bulk molecules and A_{hkl} is the area of the 2D surface cell. The thickness of the *hkl* slabs was progressively increased until the γ_{hkl} value reached convergence.

3. METHODOLOGY

In this study, we used the PBC analysis, in the sense of Hartman and Perdok,[9−11] which essentially consists of localizing [*uvw*] crystallographic directions characterized by strong interactions between growth units (represented by molecules in our case). Such directions determine the character of the {*hkl*} forms, influencing in this way the morphology of a crystal.[10] It is worth recollecting that the character of a {*hkl*} form can be defined as F (flat), when at least two PBCs run in a slice of thickness d_{hkl} allowed by the extinction rules; S (stepped), if only a PBC runs within a d_{hkl} slice; K (kinked), when no PBC can be found in the d_{hkl} slice.

Our computational path is developed as follows:

1. Evaluating the Molecular Interactions within the Crystal Bulk. This is achieved by coupling the CSEHP code and the UNI force field. CSEHP allows us to quantify the weak van der Waals interactions among pairs of molecules and to identify the [*uvw*] directions joining their centers of mass. These energy values, once evaluated, can be graded in different orders of magnitude ("bond orders" hereafter) starting from the most attractive interaction. Concerning tetracene crystal, morphologies were drawn by considering only the first two bond orders:

- First bond order, from the strongest interaction down to the one representing 10% of the highest interaction energy;
- Second bond order, from 10% down to 1% of the highest interaction energy.

On this ground, it is possible to build a bond order graph, that is, a simplified representation of the crystal structure in which small spheres stand for the molecules and lines connecting the spheres represent molecular interactions.

2. Evaluating the PBCs in the Crystal Structure. Starting from the "bond order graph" two steps assisted by molecular graphics programs allowed us to

i) verify the existence of PBCs along the directions identified by strong molecular bonds and obeying the criterion that every PBC has to be made of repetitive stoichiometric units and cannot have a dipole moment perpendicular to its own development axis;

ii) look for those PBCs built by more than one strong interaction; in this case, the direction of the PBC does not coincide with that of the bonds.

Once all the likely PBCs are detected, ECEs are calculated by means of CSEHP, after which a hierarchy based on the ECE order of magnitude is made (from now on "PBC rank").

3. Classifying the {*hkl*} Forms According to Their Character and Calculating Surface and Attachment Energies. All {*hkl*} forms that originate from the PBCs just identified must be classified as F, S, or K. Therefore, starting from the first PBC rank, F_1, S_1, and K_1 forms appear, followed by lower ranks, $F_2/S_2/K_2$, $F_3/S_3/K_3$, etc.

Then, the specific surface energies are calculated by means of the chosen potentials. Finally, utilizing the Gibbs−Wulff's

Table 1. The Molecular Interactions Issued from the First Two Bond Orders in Tetracene[a]

bond order	molecule label	molecule label	distance [Å]	direction	interaction [kJ/mol]	bond label
1	1	2	4.773	[1 $\bar{1}$ 0]	−41.6	a
1	1	2	5.125	[1 1 0]	−39.1	b
1	1	1	6.057	[1 0 0]	−25.7	c
1	1	2	12.192	[1 1 $\bar{2}$]	−6.0	d
1	1	1	13.436	[1 1 $\bar{1}$]	−5.1	e
1	1	2	13.308	[3 1 $\bar{2}$]	−4.4	f
2	1	1	7.838	[0 1 0]	−3.1	g
2	1	1	12.553	[1 0 $\bar{1}$]	−1.7	h
2	2	2	13.612	[0 1 $\bar{1}$]	−1.3	i
2	1	2	9.626	[3 $\bar{1}$ 0]	−1.3	j
2	1	2	10.155	[3 1 0]	−1.1	k
2	1	1	13.010	[0 0 1]	−0.7	l
2	1	2	15.151	[1 3 $\bar{2}$]	−0.4	m

[a] The calculations were performed by means of program-potential CSEHP-UNI.

Table 2. PBC End Chain Energies (ECE) Limited to the First Bond Order Falling into Two PBC Ranks[a]

PBC	PBC rank	bonds	ECE [erg/molecule]
[1 0 0]*	1	a + b	-1.11×10^{-12}
[1 1 $\bar{1}$]*	1	b + d	-4.27×10^{-13}
[0 1 0]	1	a + b	-4.02×10^{-13}
[1 $\bar{1}$ 0]*	1	a	-3.66×10^{-13}
[0 0 1]	1	b + d	-3.57×10^{-13}
[1 1 0]*	1	b	-3.43×10^{-13}
[1 0 $\bar{1}$]	2	a + d	-7.97×10^{-14}
[0 1 $\bar{1}$]	2	a + d	-6.91×10^{-14}
[1 1 $\bar{2}$]*	2	d	-5.00×10^{-14}
[2 1 $\bar{2}$]	2	d + f	-5.00×10^{-14}
[2 0 $\bar{1}$]	2	a + f	-4.39×10^{-14}
[3 1 $\bar{2}$]*	2	f	-3.70×10^{-14}
[2 1 $\bar{1}$]	2	b + f	-1.88×10^{-14}

[a] Directions corresponding to first order molecular bonds are marked with an asterisk. The "bonds" column shows the name of the intermolecular bonds forming the PBCs.

dx.doi.org/10.1021/cg200924m |*Cryst. Growth Des.* 2011, 11, 4639–4646

Table 3. Specific Surface Energies of the 25 Crystallographic Forms Determined by the First Bond Order of Tetracene[a]

		UNI	UFF			MM3		
character	form	$\gamma_{unrelaxed}$	$\gamma_{unrelaxed}$	$\gamma_{relaxed}$	Δ_{UR} (%)	$\gamma_{unrelaxed}$	$\gamma_{relaxed}$	Δ_{UR} (%)
F_1	{0 0 1}*	81.7	83.3	82.6	−0.8	73.5	72.0	−2.0
F_1	{1 1 2}*	123.8	122.4	119.3	−2.5	118.0	114.1	−3.3
F_1	{1 $\bar{1}$ 0}*	125.8	126.1	123.0	−2.5	119.0	115.1	−3.3
F_1	{0 1 1}*	126.6	125.2	123.3	−1.5	116.7	114.3	−2.1
F_1	{0 1 0}*	143.1	141.4	138.8	−1.8	129.2	126.3	−2.2
S_1	{1 1 0}*	150.8	151.9	146.6	−3.5	138.5	132.5	−4.3
F_1	{1 0 1}	149.9	156.8	149.7	−4.5	139.9	136.2	−2.6
F_1	{1 0 0}	162.8	171.3	166.2	−3.0	149.2	145.4	−2.5
F_2	{0 2 1}*	128.6	126.3	124.3	−1.6	117.2	114.5	−2.3
S_2	{1 1 3}	125.7	128.2	126.2	−1.6	119.5	116.3	−2.7
S_2	{2 2 3}	131.1	130.4	127.0	−2.6			
S_2	{2 $\bar{2}$ 1}	129.7	131.1	128.7	−1.8	122.6	118.7	−3.2
F_2	{1 $\bar{1}$ 1}*	130.3	132.0	129.6	−1.8	122.1	118.5	−2.9
F_2	{1 1 1}*	134.9	134.2	130.1	−3.1	125.5	120.9	−3.7
S_2	{$\bar{1}$ 3 1}	136.7	135.3	133.2	−1.6	127.6	125.2	−1.9
S_2	{1 3 3}	137.5	135.8	133.5	−1.7	128.5	125.3	−2.5
S_2	{$\bar{1}$ 1 1}*	134.8	137.5	133.7	−2.8	125.8	122.1	−2.9
F_2	{1 2 2}	141.4	140.0	134.7	−3.8	132.2	128.6	−2.7
F_2	{1 $\bar{2}$ 0}	139.3	138.7	136.4	−1.7	130.4	127.5	−2.2
S_2	{1 $\bar{3}$ 0}	140.8	140.0	137.5	−1.8	131.1	128.1	−2.3
S_2	{1 3 2}	143.6	141.6	138.0	−2.5	133.2	129.2	−3.0
S_2	{1 $\bar{1}$ 2}	136.1	141.5	138.6	−2.0	127.2	123.4	−3.0
S_2	{2 0 3}	147.4	156.1	152.1	−2.6			
F_2	{1 0 2}	147.7	157.5	154.4	−2.0	138.3	135.4	−2.1
S_2	{2 0 1}	154.8	162.9	158.4	−2.8	143.3	139.6	−2.6

[a] The γ values are expressed in erg/cm^2 and ordered by PBC rank and relaxed values obtained by UFF. Asterisks mark forms that enter the final equilibrium shape. The boxes with no results indicate calculations that did not converge.

construction, the corresponding crystal equilibrium shapes are obtained. GULP-UFF and TINKER-MM3 programs/potentials allowed us to deal with surface relaxation to produce more realistic morphologies to be compared to the unrelaxed ones. By means of CSEHP-UNI and GULP-UFF, attachment energies (E_{att}^{hkl}) can be evaluated as well, by which approximate linear growth rates (R^{hkl}) of the crystal forms can be estimated, according to the following relation:[24]

$$R^{hkl} \propto E_{att}^{hkl}$$

Quantifying the specific edge energies is another peculiarity of CSHEP that allows to verify the stability of a $[uvw]$ step and predict the morphology of the 2D islands or growth spirals on the most important crystallographic forms.

4. RESULTS AND DISCUSSION

Starting from the tetracene crystal structure (space group $P\bar{1}$, a_0 = 6.056, b_0 = 7.838, c_0 = 13.010 Å, α = 77.13, β = 72.12, γ = 85.79°; Z = 2),[25] we preliminarily quantified the interactions among the molecules of the primitive unit cell and those belonging to the first and second neighboring cells. Figure 1 shows the reference first and second bond order graph for tetracene. The color of the spheres indicates the two nonsymmetry related molecules (labeled 1 and 2 in the tables) of the asymmetric unit. The bonds of interest are sketched with colored lines and named in descending energetic and alphabetic order (Table 1).

4.1. The Equilibrium Morphology. All the energy values were classified according to their order of magnitude, by taking the strongest bond in the structure as a landmark. In the case of tetracene, the strongest interaction is equal to −41.6 kJ/mol and is the bond between molecules 1 and 2 along the $[1\bar{1}0]$ direction. As a consequence, the first bond order contains values in the range between −41.6 and −4.2 kJ/mol, the second bond order spans the interval between −4.2 and −0.4 kJ/mol, and so on. In this work, we chose to model first the equilibrium shapes resulting from the first bond order only and then those from the first plus the second bond order. In detail, the first and the second bond orders include 6 and 7 interactions, respectively (see Table 1).

4.1.1. The First Bond Order. When considering the first order intermolecular bonds, there are 13 PBCs in the tetracene structure, 6 matching strong molecular directions and 7 arising from a composition of more bonds. In Table 2, the ECE of these PBCs calculated with CSEHP are reported; they comprise two PBC ranks: six chains in the first rank and seven in the second one.

Eight crystallographic forms are generated by the 6 PBCs of the first rank. In detail, they all are F_1 except the {110} which has S_1 character. The 7 PBCs of the second rank generate 17 forms, 6 being F_2 while the remaining 11 are S_2. Table 3 shows these 25 forms classified and ordered according to their PBC rank and

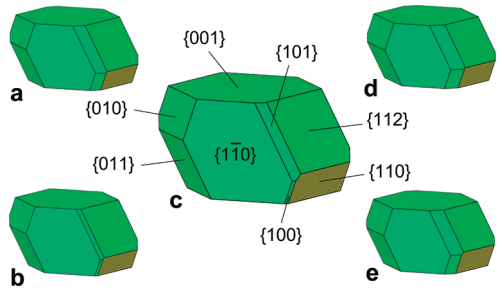

Figure 2. Tetracene equilibrium shape from the first PBC rank. The shape does not change upon extending the calculation to the second bond order. Crystal morphologies were obtained with calculations based on (a) UNI, (b) UFF without and (c) with surface relaxation, (d) MM3 without and (e) with surface relaxation.

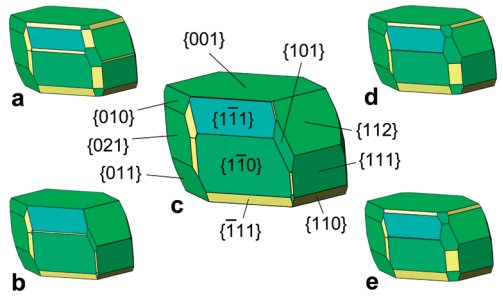

Figure 3. Tetracene equilibrium shape from the first plus the second PBC rank. Crystal morphologies were obtained with calculations based on (a) UNI, (b) UFF without and (c) with surface relaxation, (d) MM3 without and (e) with surface relaxation. Miller indexes are reported only for the crystallographic forms having MRI ≥ 1.0%.

surface energy. A fairly good agreement is evident comparing values obtained with different force fields: the UNI and UFF potentials give surface energies in close agreement, while the MM3 force field originates slightly lower γ values. The energy difference percentage

$$\Delta_{UR} = (\gamma^{relaxed} - \gamma^{unrelaxed})/\gamma^{unrelaxed}$$

between relaxed and unrelaxed surfaces is also indicated in the UFF and MM3 columns for all forms. It is worth outlining the weak relaxation suffered in general by the surfaces of tetracene crystal: indeed, Δ_{UR} goes from minima of 0.8% for UFF and 2.0% for MM3 for the {001} form, to a maximum difference always below 5%. The average Δ_{UR} are in good agreement, being 2.3% and 2.7% for UFF and MM3, respectively.

For quantitatively describing crystal morphologies, we evaluated the morphological relevance index (MRI) for all {*hkl*} forms, defined as the percent ratio between the total area of the faces belonging to a {*hkl*} form and the total surface area of the crystal. The {*hkl*} forms in Table 3 marked with an asterisk are forms having MRI ≥ 1.0% that enter the final equilibrium morphology, irrespective of the adopted force field and surface relaxation. Color coding of faces (green for F, yellow for S, and red for K faces) in Figures 2 and 3 clearly outlines that all forms (but the {110}) belonging to the first PBC rank exhibit an F character. When also the second PBC rank is considered, new F forms appear together with a few narrow S forms sitting between F faces; this result of the PBC analysis is more evident with the UNI force field (Figure 3a). Apart from minor differences (such

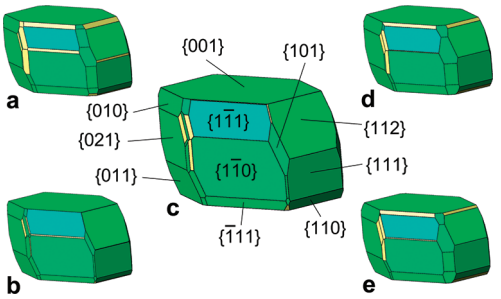

Figure 4. Tetracene equilibrium shape from the second bond order interaction including the second PBC rank. The models are derived from calculations based on (a) UNI, (b) UFF without and (c) with surface relaxation, (d) MM3 without and (e) with surface relaxation. Miller indexes are reported only for the crystallographic forms having MRI ≥ 1.0%.

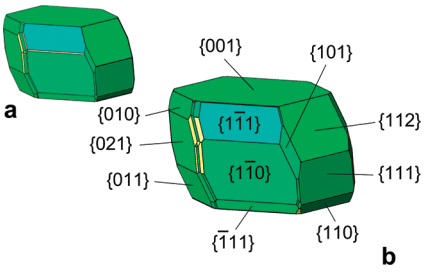

Figure 5. Tetracene equilibrium shape from the second bond order and considering the third rank of the PBCs. The crystal shapes are from calculations performed by means of UFF potentials without (a) and with surface relaxation (b). Miller indexes are reported for the crystallographic forms having MRI ≥ 1.0%.

as the smoothing of the edges between the main F forms), simulations performed with different force fields lead to morphologies that are very similar for both the index and the relative surface area of the faces.

4.1.2. The Second Bond Order. When also the second bond order is taken into account, 7 new molecular interactions, ranging between −4.2 and −0.4 kJ/mol, enter the ECE calculation. Thus, 14 more PBCs (see Table S1, Supporting Information) join the previous ones, and new 84 crystallographic forms appear.

When the second bond order is considered, two new PBCs ([101] and [210]) enter the second PBC rank: as a consequence, the first PBC rank is still associated with 8 forms, while those determined by the second PBC rank increase from 17 to 27. It is worth pointing out that a {*hkl*} form can change its character if higher bond orders are taken into account; this is the case of {110} that switches to F_1 from S_1 on moving from the first to the second bond order. Table S2, Supporting Information resumes the first two PBC ranks obtained from the first two bond orders. Comparing Table S2, Supporting Information with Table 3, the S_2 faces ($\bar{1}$11), ($\bar{1}$31), (133), (1$\bar{3}$0), (132), (201) and (203) change their character to F_2.

A first evidence ensues: the crystal equilibrium shape obtained from the first PBC rank does not change with the bond order considered (see Tables 3 and S2 and Figure 2).

The overall 109 forms are completed by the appearance of faces belonging to the third (69) and to the fourth (5) PBC rank. We limited our calculations to γ values associated with the third PBC rank that, given the good agreement among the three different force fields, were solely studied by the UFF potentials (Table S3,

dx.doi.org/10.1021/cg200924m |*Cryst. Growth Des.* 2011, 11, 4639–4646

Table 4. The MRI ≥ 1.0% for Each Calculation Class under Consideration (Upper) and Total MRI Referred to PBC Rank and Character of the Faces (Lower)[a]

MRI (%)	38.7 {001} 20.0 {1 1̄ 0} 16.6 {112} 9.8 {011} 7.8 {010} 5.8 {110} 1.2 {101}	38.2 {001} 19.7 {1 1̄ 0} 16.0 {112} 9.6 {011} 7.8 {010} 6.4 {110} 2.1 {101}	37.9 {001} 11.8 {112} 11.7 {1 1̄ 0} 8.2 {111} 7.5 {021} 6.8 {1 1̄ 1} 5.6 {011} 2.7 {010} 1.9 {1̄ 11} 1.6 {110}	37.3 {001} 11.9 {1 1̄ 0} 11.6 {112} 8.1 {111} 7.3 {021} 6.6 {1 1̄ 1} 5.6 {011} 2.8 {010} 2.2 {1̄ 11} 2.1 {110} 1.0 {101}	37.8 {001} 11.8 {112} 11.5 {1 1̄ 0} 8.2 {111} 7.4 {021} 6.8 {1 1̄ 1} 5.4 {011} 2.6 {010} 1.8 {1̄ 11} 1.3 {110}	37.3 {001} 11.6 {112} 11.5 {1 1̄ 0} 8.1 {111} 7.2 {021} 6.4 {1 1̄ 1} 5.4 {011} 2.7 {010} 2.1 {1̄ 11} 2.1 {110} 1.0 {101}	37.8 {001} 11.6 {112} 11.5 {1 1̄ 0} 8.2 {111} 7.1 {021} 6.8 {1 1̄ 1} 5.0 {011} 2.4 {010} 1.8 {1̄ 11} 1.3 {110}	37.2 {001} 11.6 {1 1̄ 0} 11.1 {112} 8.0 {111} 6.9 {021} 6.4 {1 1̄ 1} 4.7 {011} 2.5 {010} 2.0 {1̄ 11} 2.0 {110} 1.0 {101}
bond order	1st (2nd)	1st (2nd)	1st	1st	2nd	2nd	2nd	2nd
PBC rank	1st	1st	2nd	2nd	2nd	2nd	3rd	3rd
relaxation	no	yes	no	yes	no	yes	no	yes
PBC 1	100.0%	100.0%	71.8%	72.4%	71.0%	71.7%	70.1%	70.1%
PBC 2	-	-	28.2%	27.6%	29.0%	28.3%	27.3%	26.3%
PBC 3	-	-	-	-	-	-	2.6%	3.6%
F	94.2% (100%)	93.6% (100%)	92.8%	92.7%	98.7%	98.9%	97.8%	97.5%
S	5.8% (0%)	6.4% (0%)	7.2%	7.3%	1.3%	1.1%	2.2%	2.5%
K	0.0%	0.0%	0.0%	0.0%	0.0%	0.0%	0.0%	0.0%

[a] All data were calculated with the UFF potentials.

Supporting Information). Among the new forms pertaining to the third PBC rank, we noticed a preponderance of S faces plus few K faces that do not enter the final equilibrium shape. In the second bond order, the average relaxation percentage is as low as that found in the first; it reaches a value of 2.3%, with negligible discrepancies among F (2.4%), S (2.2%), and K (2.5%) forms.

Figure 5 shows the most complete equilibrium shapes we obtained: no sensible variations between the shapes obtained from the first bond order and the second PBC rank are observed. The only difference is the appearance of very small faces (MRI < 1%) which round the edges between F forms.

Table 4 reports the MRI of all forms with surface extension ≥1.0% for every calculation class explored; furthermore, the weight of the character and the pertinent PBC rank is considered as well. This table supports some important conclusions. As one could expect, the forms arising from the first PBC rank and those with F character control the final morphologies, their MRI definitely remaining above 70% and 90%, respectively. In detail, the F character gains weight if the bond class increases, while slightly reduces with the PBC rank.

4.2. The Growth Form. The modeling tools discussed here allowed us to calculate the E_{att}^{hkl} relative to the crystallographic forms presented in the previous paragraphs. Table S4, Supporting Information shows the E_{att}^{hkl} values estimated by UFF.

Surface relaxation brings E_{att}^{hkl} changes:

$$\Delta_{EAR} = (E_{att}^{relaxed} - E_{att}^{unrelaxed})/E_{att}^{unrelaxed}$$

even lower than Δ_{UR}; the mean value is 1.2% with small discrepancies among F (1.0%), S (1.4%), and K (1.1%) forms. Notably, the crystallographic form which is least modified by introducing surface relaxation is again {001} showing Δ_{EAR} = 0.04%. This is easily understood in terms of crystal structure since the d_{001} slice contains the highly compact herringbone packing motif typical of most organic semiconductors belonging to the families of oligoacenes, oligothiophenes, and oligophenylenes. Moreover, surface relaxation may cause a small increase of E_{att}^{hkl} for some faces, hence giving rise to negative values of Δ_{EAR}.

Figure 6a,b gives evidence of the growth shapes (GS) corresponding to E_{att}^{hkl} values in Table S4, Supporting Information; Figure 6c refers to UNI force field simulations whose results are collected in Table S5, Supporting Information. As it can be noticed, the growth habit is fairly different from the equilibrium one: it is tabular and dominated by the {001} form. Besides, the number of GS forms is remarkably smaller with respect to the ES, since no rounding of crystal edges occurs. The seven forms that enter the final growth morphology are the following: {001}, {101}, {011}, {010}, {111}, {1$\bar{1}$0}, and {112}, all possessing F

dx.doi.org/10.1021/cg200924m |Cryst. Growth Des. 2011, 11, 4639–4646

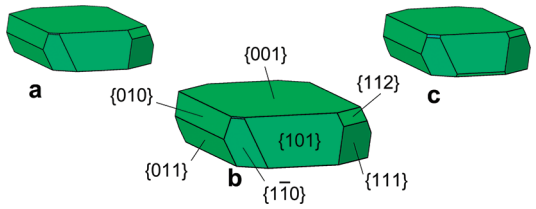

Figure 6. Tetracene growth shapes simulated by means of (a) UFF without (b) and with surface relaxation, and (c) UNI potentials.

character. Their MRI, including surface relaxation, becomes 61.4, 10.5, 10.2, 8.4, 4.7, 3.5, and 1.3%, respectively. Their d_{hkl} layers include the strongest PBCs, namely, [100], [11$\bar{1}$], [010], [1$\bar{1}$0], [001], and [110]. This means that the theoretical growth shape is yet well represented when the sole molecular interactions of the first order of magnitude are taken into account, as is commonly found in the literature.

These results completely agree with the growth shape simulated by Cuppen and co-workers[6] who utilized the Dreiding force field in combination with ESP derived point charges. In the same paper, an experimental growth morphology is reported: the tetracene crystals, grown from vapor, show a tabular habit strongly dominated by the {001}. To our knowledge, this is the only paper that reports the face indexing of an experimentally grown single crystal, the great majority of the papers concerning the deposition of thin films and nanoaggregates.

5. CONCLUSIONS

First of all, we have to underline the excellent agreement among the three force fields employed in this work. In more detail, we have to note a better concordance between values obtained by UNI and UFF, while energy values from the MM3 calculations are slightly lower, on average.

The ensemble of our results for this case study led us to argue that the equilibrium morphology of organic crystals has to be faced with great care. The a priori exclusion of forms with complex indexes can produce big errors when predicting the mean γ value that enters the relations used to determine both 3D and 2D nucleation frequency.[26] Moreover, disregarding the existence of such forms could definitely cause a deficit of information for evaluating the adsorption of both solvent and impurities.

Unlike ionic structures, these molecular phases are characterized by a relevant number of stable PBCs: no chains exist with repulsive ECE because all the molecules can establish a bond among themselves. As a consequence, apart from the {001}, this kind of crystal has many forms with similar specific surface energies, that is to say, an equilibrium shape rich in faces. This implies that the equilibrium morphology is strongly influenced by the point group. To confirm this, we have preliminary similar results with another oligoacene, namely, pentacene, as it will be shown in a forthcoming paper.

In the case of tetracene a nearly barrel habit is produced: one form, the {001}, rules over the other ones and several faces roughly belong to the zone axis perpendicular to the dominant form. This is not surprising since four out of the six first rank PBCs (i.e., [100], [010], [1$\bar{1}$0], [110]) run within a slice of d_{001} thickness. Some edges are more and more rounded increasing both the bond order and the PBC rank; we foresee that the rounding level of the edges could slightly increase after taking into account the third bond order and the fourth PBC rank and so on, nevertheless leaving the general shape basically unmodified.

Concerning the character of the surfaces, we can conclude that the F faces largely dominate both the equilibrium and the growth morphologies. Only a few small S faces (about 2.5% of the total surface area) touch the edges between F ones, while no K faces appear in the final shape. This perfectly agrees with Hartman's thought[27] about the character of the crystallographic forms in nonionic crystals that turns out to be reasonable and fully valid until now, even if faced with modern calculation facilities and greatly improved intermolecular force fields.

Another relevant result emerging from the present paper is the observation that surface relaxation in general weakly affects surface and attachment energies of molecular crystals; being confident of this general behavior (which is apparently broken in only very few cases,[28,29] the crystal shapes do not significantly differ from those predicted by simply cutting the bulk structures. The same result is also of relevance for simulation of organic−organic epitaxial systems and evaluation of epitaxial relations and adhesion energies.[30−33] This behavior somewhat differs from what observed with ionic structures. As a matter of fact, we demonstrated in previous works[34−37] that relaxation strongly affects calcite and gypsum surfaces. In the case of calcite the {0001}, {01$\bar{1}$2}, and {10$\bar{1}$0} forms enter the final equilibrium shape (in a vacuum at 0 K) thanks to the geometry optimization of surfaces, without which only the {10$\bar{1}$4} rhombohedron could appear. For what concerns gypsum, apart from the stable {010}, every face suffers a relaxation of at least 25−30% with a significant modification of the final equilibrium shape.

One of the main goals of the present study lies in providing information to people who intend to simulate equilibrium and growth morphologies of molecular crystals. We propose a methodology which represents a compromise between the time of calculation and the reliability of the results. Our calculations, at least about tetracene, prove that, for the equilibrium shape, it is sufficient to consider the molecular interactions belonging to the first order of magnitude (with all the related PBC ranks), being aware that a few minor faces could originate from calculations in range of the second order. Concerning a reasonable evaluation of the growth shape, we prove that it is sufficient to consider the strongest PBCs in the structure, that is, those from the first bond order.

Obviously, we do not believe that these conclusions are valid for the totality of the known organic phases, but we think they could have implications on molecular systems similar to tetracene, in particular, on the other members of the oligoacenes class, about which an analogous study is underway.

■ ASSOCIATED CONTENT

Supporting Information. The molecular structure of the six PBCs belonging to the first PBC rank, tables listing the ECE of the PBCs belonging to the second bond order, and specific surface energies and attachment energies of the forms included in the first three PBC ranks, considering the first two bond orders. This material is available free of charge via the Internet at http://pubs.acs.org.

■ AUTHOR INFORMATION

Corresponding Author

*E-mail: roberto.massaro@mater.unimib.it.

REFERENCES

(1) Witte, G.; Wöll, C. *J. Mater. Res.* **2004**, *19*, 1889–1916.
(2) de Boer, R. W. I.; Gershenson, M. E.; Morpurgo, A. F.; Podzorov, V. *Phys. Status Solidi* **2004**, *201*, 1302–1331.
(3) Reese, C.; Bao, Z. *J. Mater. Chem.* **2006**, *16*, 329–333.
(4) Anthony, J. E. *Angew. Chem. Int. Ed.* **2007**, *46*, 452–483.
(5) Northrup, J. E.; Tiago, M. L.; Louie, S. G. *Phys. Rev. B* **2002**, *66*, 121404.
(6) Cuppen, H. M.; Graswinckel, W. S.; Meekes, H. *Cryst. Growth Des.* **2004**, *4*, 1351–1357.
(7) Drummy, L. F.; Miska, P. K.; Alberts, D.; Lee, N.; Martin, D. C. *J. Phys. Chem. B* **2006**, *110*, 6066–6071.
(8) Nabok, D.; Puschnig, P.; Ambrosch-Draxl, C. *Phys. Rev. B* **2008**, *77*, 245316.
(9) Hartman, P.; Perdok, W. G. *Acta Crystallogr.* **1955**, *8*, 49–52.
(10) Hartman, P.; Perdok, W. G. *Acta Crystallogr.* **1955**, *8*, 521–525.
(11) Hartman, P.; Perdok, W. G. *Acta Crystallogr.* **1955**, *8*, 525–529.
(12) Aquilano, D.; Rubbo, M.; Catti, M.; Pavese, A. *J. Cryst. Growth* **1997**, *182*, 168–184.
(13) Rubbo, M.; Aquilano, D. *J. Cryst. Growth* **1998**, *194*, 156–159.
(14) Filippini, G.; Gavezzotti, A. *Acta Crystallogr. B* **1993**, *49*, 868–880.
(15) Gavezzotti, A. *Molecular Aggregation: Structure Analysis and Molecular Simulation of Crystals and Liquids*; Oxford University Press: New York, 2007.
(16) Rappé, A. K.; Casewit, C. J.; Colwell, K. S.; Goddard, W. A., III; Skiff, W. M. *J. Am. Chem. Soc.* **1992**, *114*, 10024–10035.
(17) Gale, J. D. *J. Chem. Soc. Faraday Trans.* **1997**, *93*, 629–637.
(18) Dovesi, R.; Civalleri, B.; Orlando, R.; Roetti, C.; Saunders, V. R. In *Reviews in Computational Chemistry*; Lipkowitz, B. K.; Larter, R.; Cundari, T. R., Eds.; John Wiley and Sons Inc.: New York, 2005; Vol. 21, pp 1−125.
(19) Gale, J. D. *General Utility Lattice Program User's Manual*; Curtin University of Technology: Perth, Australia.
(20) Kern, R. In *Morphology of Crystals Part A*; Sunagawa, I., Ed.; Terra Scientific Publishing Co.: Tokyo, 1987; pp 77−206.
(21) Allinger, N. L.; Yuh, Y. H.; Lii, J.-H. *J. Am. Chem. Soc.* **1989**, *111*, 8551–8566.
(22) Lii, J.-H.; Allinger, N. L. *J. Am. Chem. Soc.* **1989**, *111*, 8566–8575.
(23) Ponder, J. W. *Tinker, Software Tools for Molecular Design*, Version 4.2, June 2004.
(24) Hartman, P.; Bennema, P. *J. Cryst. Growth* **1980**, *49*, 145–156.
(25) Holmes, D.; Kumaraswamy, S.; Matzger, A. J.; Vollhardt, K. P. C. *Chem.—Eur. J.* **1999**, *5*, 3399–3412.
(26) Mutaftschiev, B. *The Atomistic Nature of Crystal Growth*; Springer-Verlag: Berlin, 2001; pp 223−248.
(27) Hartman, P. *Acta Crystallogr.* **1958**, *11*, 459–464.
(28) Hastie, G. P.; Johnstone, J.; Walker, E. M.; Roberts, K. J. *J. Chem. Soc. Perkin Trans. 2* **1996**, 2049–2050.
(29) Overney, R. M.; Howald, L.; Frommer, J.; Meyer, E.; Brodbeck, D.; Güntherodt, H. J. *Ultramicroscopy* **1992**, *42−44*, 983–988.
(30) Haber, T.; Resel, R.; Thierry, A.; Campione, M.; Sassella, A.; Moret, M. *Physica E* **2008**, *41*, 133–137.
(31) Campione, M.; Moret, M.; Raimondo, L.; Sassella, A. *J. Phys. Chem. C* **2009**, *113*, 20927–20933.
(32) Campione, M.; Raimondo, L.; Moret, M.; Campiglio, P.; Fumagalli, E.; Sassella, A. *Chem. Mater.* **2009**, *21*, 4859–4867.
(33) Raimondo, L.; Moret, M.; Campione, M.; Borghesi, A.; Sassella, A. *J. Phys. Chem. C* **2011**, *115*, 5880–5885.
(34) Bruno, M.; Massaro, F. R.; Prencipe, M. *Surf. Sci.* **2008**, *602*, 2774–2782.
(35) Bruno, M.; Massaro, F. R.; Prencipe, M.; Aquilano, D. *CrystEngComm* **2010**, *12*, 3626–3633.
(36) Massaro, F. R.; Bruno, M.; Aquilano, D. *Cryst. Growth Des.* **2010**, *10*, 4096–4100.
(37) Massaro, F. R.; Rubbo, M.; Aquilano, D. *Cryst. Growth Des.* **2010**, *10*, 2870–2878.